Multiple-samples-method enabling high dynamic range imaging for high frame rate CMOS image sensor by FPGA and co-processor

Blake C. Jacquot*, Nathan Johnson-Williams
The Aerospace Corporation, 2310 E. El Segundo Blvd., El Segundo, CA 90245-4609

ABSTRACT

We present results from a prototype CMOS camera system implementing a multiple sampled pixel level algorithm ("Last Sample Before Saturation") to create High-Dynamic Range (HDR) images that approach the dynamic range of CCDs. The system is built around a commercial 1280 × 1024 CMOS image sensor with 10-bits per pixel and up to 500 Hz full frame rate with higher frame rates available through windowing. We analyze imagery data collected at room temperature for SNR versus photocurrent, among other figures of merit. Results conform to expectations of a model that uses only dark current, read noise, and photocurrent as input parameters.

Keywords: CMOS image sensor, wide dynamic range, day/night vision, CIS, SNR, FPGA

1. INTRODUCTION

1.1 Motivation

CMOS imagers are becoming the dominant visible image sensor for space-based applications as the CCD industrial base declines. The slow CMOS adoption relative to other industries is driven largely by CCDs having characteristics that fit well with space surveillance needs. Such capabilities include time delay and integrate (TDI), low fixed pattern noise (FPN), and high dynamic range. The generally lower dynamic range of CMOS imagers can be partly addressed by techniques and algorithms for High/Wide Dynamic Range CMOS (HDR/WDR). Though algorithmic HDR approaches are used in some high-volume commercial CMOS imager applications, these techniques have not yet been widely deployed for space systems.

Implementing real-time algorithms for high dynamic range operation requires significant computing power. The system must capture, analyze, and store every pixel according to the constraints of the algorithm without dropping frames. A FPGA or ASIC front end can be used to reduce computational load on the host processor, but the challenge is still daunting.

1.2 Contributions

This paper documents use of the multiple samples technique to extend the dynamic range for a commercial CMOS image sensor as part of a path to a high-speed camera module capable of real-time image processing. Though used in ground-based applications, this technique is new to space systems, which typically use electron well capacity adjustment for dynamic range extension. The multiple samples technique (in model form) allows arbitrarily large dynamic range with appropriately scaled computational demands.

1.3 Related Work

There are roughly eight commonly-used ways to enable HDR in CMOS image sensors: Dual column level amplifier, Logarithmic pixel, Multiple sampled pixel, Pixel level Sigma Delta ADC with residue readout, Time to saturation with residue readout, Multiple wells, Well adjustment by adjusting reset signal, and Spatially varying exposure[1–8].

*blakejacquot@gmail.com; phone 1 310 336-1510; http://www.aerospace.org/

Optics and Photonics for Information Processing VIII, edited by Abdul A. S. Awwal, Khan M. Iftekharuddin, Mohammad A. Matin, Proc. of SPIE Vol. 9216, 921609
 · doi: 10.1117/12.2062284

An early use of a multiple sample scheme used two column parallel readouts to enable a short and long exposure[9]. Another similar implementation used dual capture[10]. A user stitched two images together to create an HDR image. This approach is not easily scalable to more than two samples due to area constraints. Other work used pixel-level analog-to-digital converters (ADC) to enable an arbitrary number of samples[11]. Later work applied multiple samples to reduce read noise at low illumination by "averaging" the captured images to reduce read noise[12]. An integrated "system-on-chip" approach enables multiple samples by including a microcontroller[13]. There is also more recent work using the multiple samples approach[14–19].

1.4 Limitations and Benefits

The main limitations of the multiple samples method are computational complexity, memory requirements, and increased power. Broadly, two different strategies can be used: HDR images can be computed in real time or, alternatively, all images can be stored to memory and post-processed. Computing HDR images in real time requires increased computational bandwidth to sample, store, and process images quickly enough to avoid data drop outs. The post processing alternative requires less computational bandwidth but much more memory as each raw image must be stored before processing can begin.

In both cases, the limiting factors are typically data throughput and total data from the image sensor. A post-processing solution requires memory bandwidth equal to or greater than the output rate of the image sensor in addition to the capacity needed to store the desired amount of raw frames. A real-time solution must have a complete system throughput greater than or equal to the data output rate from the sensor.

However, once the multiple samples method is implemented, the system naturally lends itself to running a large number of algorithms. These may allow the sensor system to transmit regular, lower-frame rate frequencies and go into burst or windowing modes if something interesting is seen (e.g. moving object).

A concern not often discussed for multiple samples is the need for good anti-blooming circuitry in the image sensor unit cell. In the absence of good anti-blooming circuitry, scenes with sharp structure will result in pixels with high illumination blooming charge into neighboring pixels with low illumination. This leads to distortions in algorithm results.

2. METHOD

2.1 Multiple Samples Approach

The multiple samples method samples and stores each pixel at higher rates than intended for the final HDR image and processes these samples according to the algorithm that is described conceptually in Figure 1. At evenly spaced intervals in time each pixel value is recorded. At the end of the frame cycle, each pixel is analyzed to determine if it has reached full well (i.e. is saturated or not). If not saturated, the last recorded value is stored for the HDR image. However, if saturated, the algorithm backtracks along the pixel samples until it finds the last sample before saturation (LSBS). With this LSBS sample and record of the origin (and possibly other unsaturated samples), the algorithm extrapolates based on a linear fit to what value the pixel would have if it did not reach full well at end-of-frame. This extrapolated value is stored for the HDR frame. After the frame time, all pixels are reset and the process repeats. This approach requires the ability to perform non-destructive readout (NDR). Further, it may work best with global shutter, in which all pixels are reset simultaneously. In theory it could be used in ripple read mode if there is no crosstalk. Furthermore, this method lends itself easily to allowing correlated double sampling (CDS) to reduce kTC reset noise.

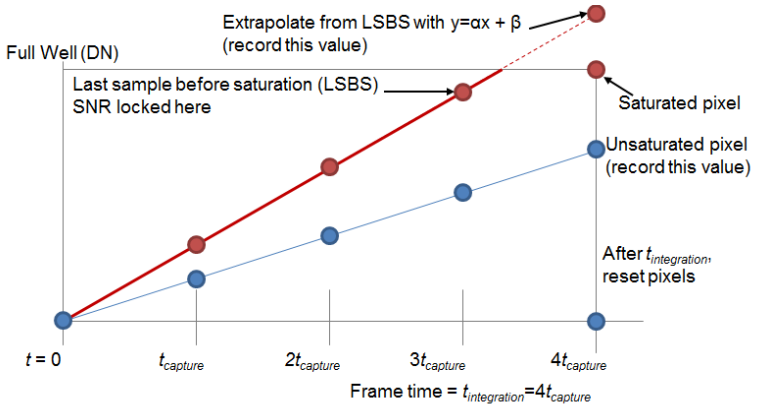

Figure 1. Conceptual representation of multiple sampled pixel method (also known as last sample before saturation).

The Signal-to-Noise Ratio (SNR) for individual pixels is determined by the last sample before saturation and is a function of integrated photocurrent (signal), integrated dark current, and read noise. There is more than one way to formulate the SNR expression when dealing with multiple samples. We found the following approach intuitive and useful for algorithm construction. Integrated photocurrent can be calculated as

$$Signal\ (e-) = \frac{i_{ph}\, m\, t_{integration}\, a}{q} \tag{1}$$

Here i_{ph} is photocurrent per unit area, a is pixel area, q is the elementary charge, and m is fraction of $t_{integration}$ used to construct HDR image. Note, $t_{integration}$ is the product of the integration time per sample ($t_{capture}$) and the total number of samples.

Noise is function of the shot noise from signal and dark current as well as read noise. It is expressed as

$$Noise\ (e-) = \sqrt{\frac{(i_{ph}+i_{dark})\, m\, t_{integration}\, a}{q} + \sigma_{read}^2} \tag{2}$$

Signal-to-noise ratio (SNR) can then be calculated as

$$SNR = \frac{Signal}{Noise} \tag{3}$$

$$SNR\ (dB) = 20\ log_{10}\left(\frac{Signal}{Noise}\right) \tag{4}$$

After determining the maximum and minimum detectable photocurrent, intrascene dynamic range (DR) can be calculated as

$$DR = \frac{i_{max}}{i_{min}} \tag{5}$$

$$DR\ (dB) = 20\ log_{10}\left(\frac{i_{max}}{i_{min}}\right) \tag{6}$$

The generally-accepted definition of i_{min} is the value for which SNR (dB) is equal to one. This value will be slightly larger than the read noise floor of the system with the excess due to shot noise of dark current. The definition of i_{max} is more open. Here, we adopt the definition of bloomed full well which is the peak available SNR for a pixel.

Variable definitions are given in Table 1.

Table 1. Definitions for variables used in equations.

Variable Definitions		
Variable	Description	Units
i_{ph}	Photocurrent	nA/cm^2
i_{dark}	Dark current	nA/cm^2
$t_{integration}$	Integration time of HDR image	sec
$t_{capture}$	Integration time image subsample	sec
a	Pixel area	cm^2
q	Elementary charge	C/e-
σ_{read}	Read noise	e-
m	Fraction of $t_{integration}$ used to construct HDR image	

With these equations, the behavior expected of the multiple samples method can be modeled and compared against measured data.

3. IMPLEMENTATION

3.1 Image Sensor

The CMOS image sensor chosen for this demonstration is the SXGA (1280 × 1024) LUPA1300-2 from ON Semiconductor in 168-Pin µPGA Package[20]. It accommodates 500 frames per second (fps) at full frame readout, but can reach 102,249 fps with extreme windowing. We chose a 216 × 400 window at 1228.4 fps for internal needs. The sensor has non-destructive readout and global shutter. Internal requirements stipulated relatively large pixel pitch and bit depth of at least 10 bits. The LUPA1300-2 is one of the few sensors meeting all requirements and also available in small purchase quantities for prototyping. Key settings and specifications for the sensor are shown in Table 2.

Table 2. Key image sensor settings and specifications.

Image Sensor Settings and Specifications			
User-Selected		Fixed	
Window width	216 pixels	Pixel pitch	14 µm
Window height	400 pixels	ADC bit depth	10 bits
Frame rate	1228.4 Hz	Pixel rate	630 Mbps per channel
$t_{capture}$	783.6 µsec	Output	Monochrome
Shutter	Global	Pixel architecture	6T
Video channels used	2	CDS	On-chip
Synch channel used	1		
Non-destructive readout	Enabled		
FPN correction	Enabled		

3.2 Sensor Programming

An Arduino Nano microcontroller drove the sensor's input serial peripheral interface (SPI) for sensor settings and programming. The Arduino was controlled via a software interface on a host PC. Commands to the sensor were issued by the host PC and then transmitted to the sensor via the Arduino. A level shifter converted the 5 V Arduino logic levels to the 3.3 V levels required by the sensor.

3.3 Data Acquisition

A Xilinx KC705 Kintex-7 FPGA development board received two serial LVDS video lines and one LVDS synch line from the image sensor. The FPGA was used to deserialize, synchronize, and transmit the image data via USB to the host PC for storage and analysis.

4. RESULTS

4.1 Performance Evaluation

We collected four captures for every HDR image and expected a corresponding fourfold dynamic range increase while maintaining a "sawtooth" SNR profile with respect to increasing photocurrent. The "sawtooth" profile arises due to the tradeoff between SNR and fraction of $t_{integration}$ used. SNR increases with integrated signal until full well is reached, at which point the algorithm chooses a smaller fraction of $t_{integration}$ that has not yet saturated. With the drop in signal, the SNR drops, but remains above the SNR for very small integrated signal levels in the longest sample.

To validate expectations and create a model, we needed to accurately measure read noise, dark current, conversion gain, and full well. These specifications were also provided by the vendor datasheet and allow a benchmark for comparison to measured data.

4.2 System Validation (Mean-Variance, Dark Current, Linearity)

Figure 2 shows a transfer curve for the sensor response under constant illumination at room temperature by varying integration time. Pixel values spanned the majority of bit depth allowed by 10-bit pixels after optimizing for gain and offset. Here, digital number (DN) is the digital count read for each pixel. Flood illumination for all tests is provided by a high-power 635 nm LED that is spatially diffused by an integrating sphere

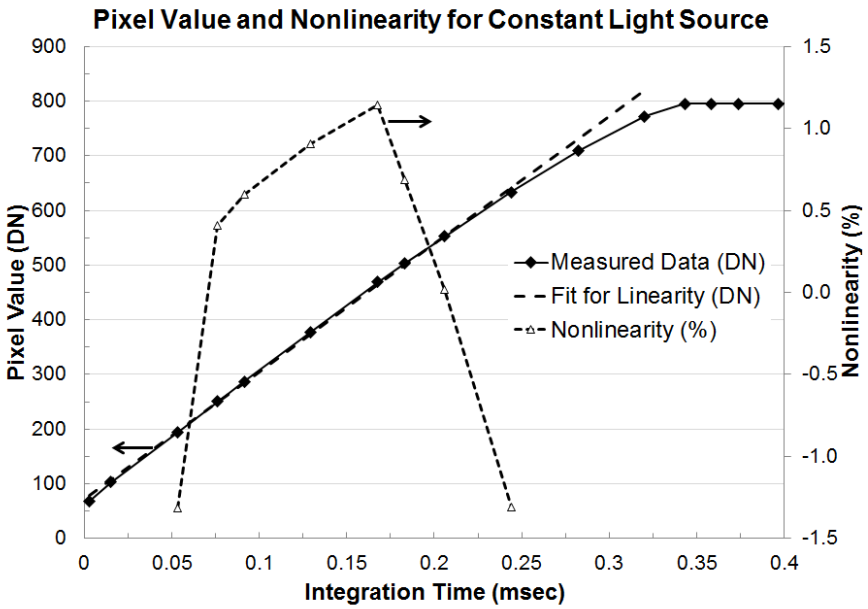

Figure 2. Transfer curve and local non-linearity of the sensor under constant illumination with varying integration time.

Integral nonlinearity (INL) is calculated as

$$Nonlinearity\ (\%) = \frac{Measured\ datapoint - Fitted\ datapoint}{Fitted\ datapoint} * 100 \quad (7)$$

With gain and offset settings selected, the system gain was directly measured with a mean-variance curve shown in Figure 3. A mean-variance curve takes advantage of shot noise statistics of impinging photons to measure conversion gain of the system in terms of electrons per digital number (e-/DN). This mean-variance curve is collected with a constant integration time of 783.6 µsec (equal to $t_{capture}$) and a varying intensity for the flood illumination source. Derivation of conversion gain extraction is given in Appendix A.

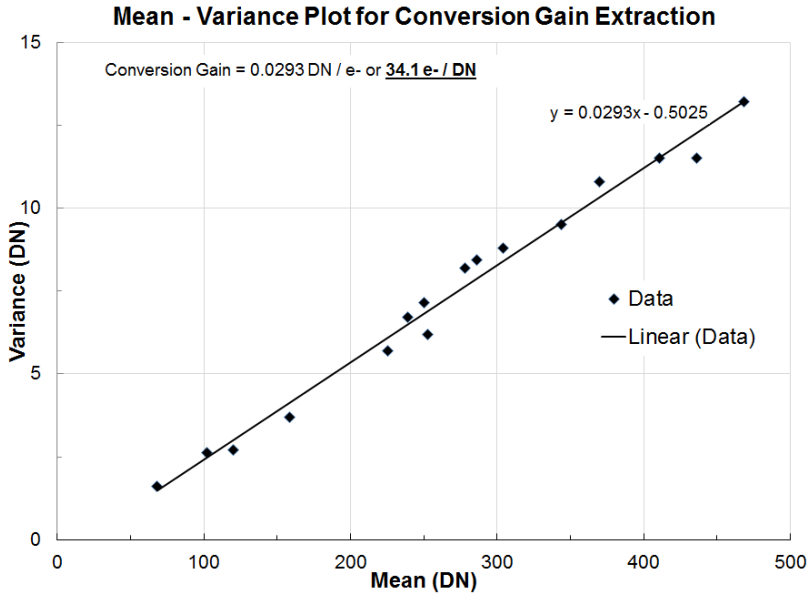

Figure 3. Mean-variance curve of sensor with constant integration time and varying illumination.

For a mean-variance curve, we can specify the theoretical mean as equal to (1) and variance as the square of (2). Note, this definition of mean-variance assumes dark current does not contribute to net signal but does contribute to noise. This is true if offset adjust is used for a given integration time.

The results of all validation measurements are presented in Table 3. Lab measurements compared favorably with vendor-provided specification.

Table 3. Lab validation measurements and corresponding values from vendor datasheet.

Image Sensor Measured and Modeled Parameters			
	Read Noise	Dark Current	Conversion Gain
Datasheet	1.2025 DN	162 DN/sec	30.769 e-/DN
Measured	1.1197 DN	200 DN/sec	34.136 e-/DN
	Read Noise	Dark Current	Full Well
Datasheet	37.0 e-	5.0 ke-/sec	30 ke-
Measured	38.2 e-	6.8 ke-/sec	21.6 ke-
			Bloomed full well measured near 632 DN = 21.6 ke
			Saturated full well measured near 900 DN = 30.7 ke-

4.3 Demonstration

Data collected using the multiple samples method is displayed with a model using measured image sensor parameters in Figure 4. Here, $t_{capture}$ is held constant while light intensity was varied. Each sample represents 783.6 µsec of integration giving 3.1344 msec HDR integration time. The associated model is calculated from three parameters: read noise, dark current, and photocurrent. Model and measured data generally agree.

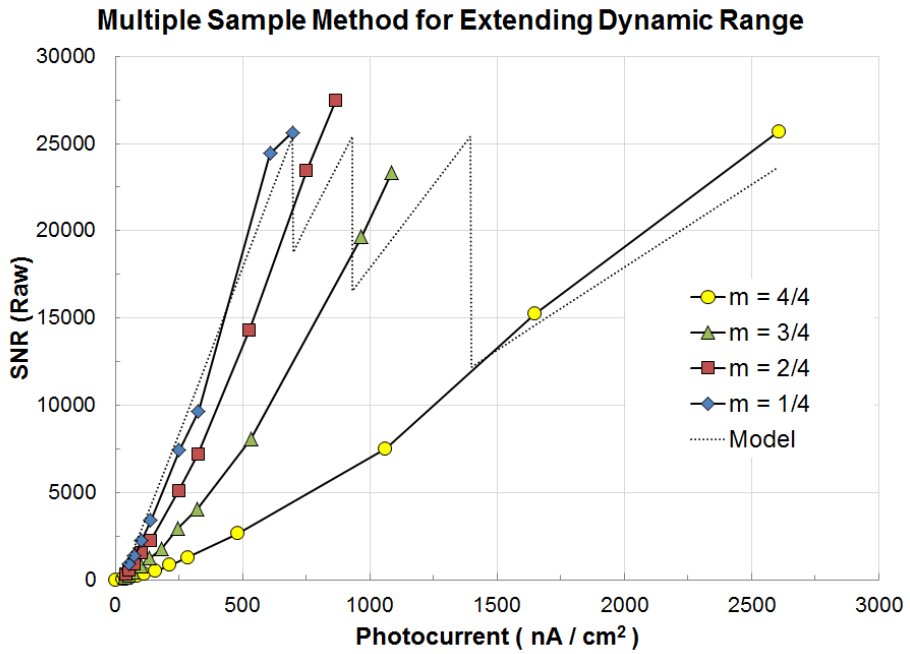

Figure 4. SNR versus photocurrent with model.

Figure 5 shows the same data in a different format. Included in this figure is the calculated maximum SNR allowed by vendor specifications, which agrees well with measured and modeled values.

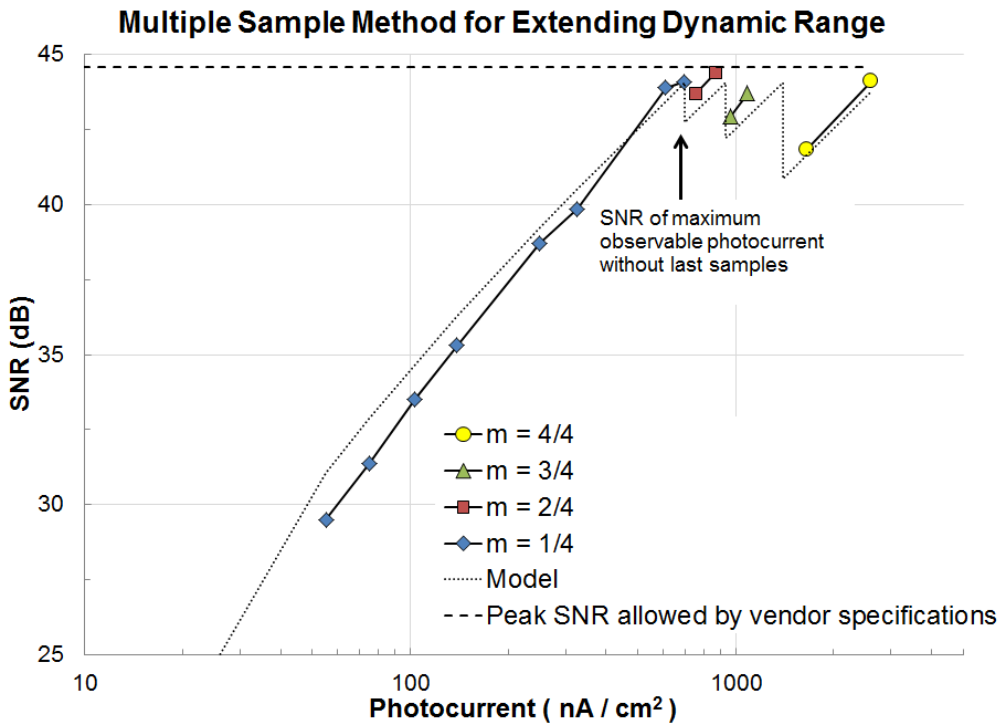

Figure 5. SNR (dB) versus photocurrent and model with maximum allowed SNR by vendor datasheets.

Tabulated results from multiple samples measurement and model are shown in Table 4. The maximum detectable signal increases by a factor of four, as expected and improves dynamic range from 56.0 dB to 68.1 dB. Included in this table is a representative dynamic range of 90.5 dB from a CCD. This large CCD dynamic range without special HDR techniques accounts for a portion of the slow adoption of CMOS imagers for space-based applications.

Table 4. Measured and modeled parameters for image sensor under test at room temperature.

Measured and Modeled Parameters

	Photocurrent (nA/cm^2)	SNR (dB)	
Min detectable signal (measured)	1.1	1.0	
Max detectable signal (measured, 1 sample)	696	44.1	
Max detectable signal (measured, 4 samples)	2789	44.1	
Max allowed by sensor datasheet (modeled)		44.6	
	Dynamic Range	**Dynamic Range (dB)**	**Note**
Dynamic range (max from datasheet, 1 sample)	810.8	58.2	37.0 e- read noise, 30 ke- full well
Dynamic range (measured, 1 sample)	632.7	56.0	i_{max} *(1 sample)* / i_{min}
Dynamic range (measured, 4 samples)	2535.5	**68.1**	i_{max} *(4 samples)* / i_{min}
Unmodified CCD with similar pixel pitch	>33333	>90.5	<3.0 e- read noise, >100 ke- full well 13.5 µm pixel

Figure 6 highlights the "sawtooth" nature of multiple samples method where SNR stays steady over extended range as well as results of a hypothetical infinite full well. An infinite full well would allow for background limited performance (BLIP) over a large range, which the multiple samples technique can't deliver.

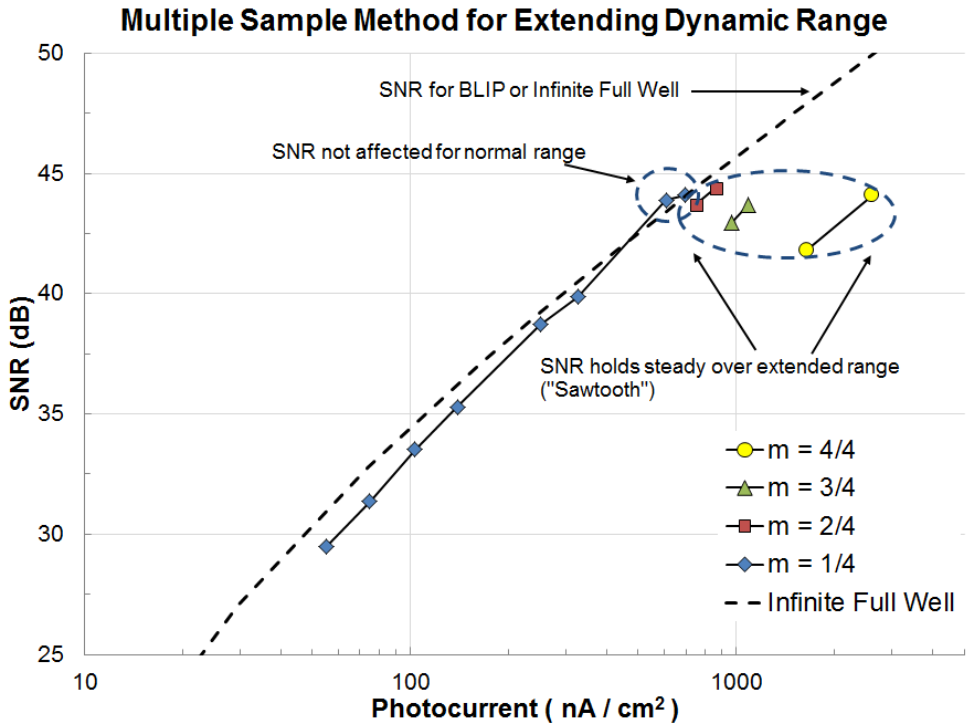

Figure 6. SNR versus photocurrent and hypothetical infinite full well.

Figure 7 summarizes HDR results by plotting dynamic range versus percentage of integration time used for image capture.

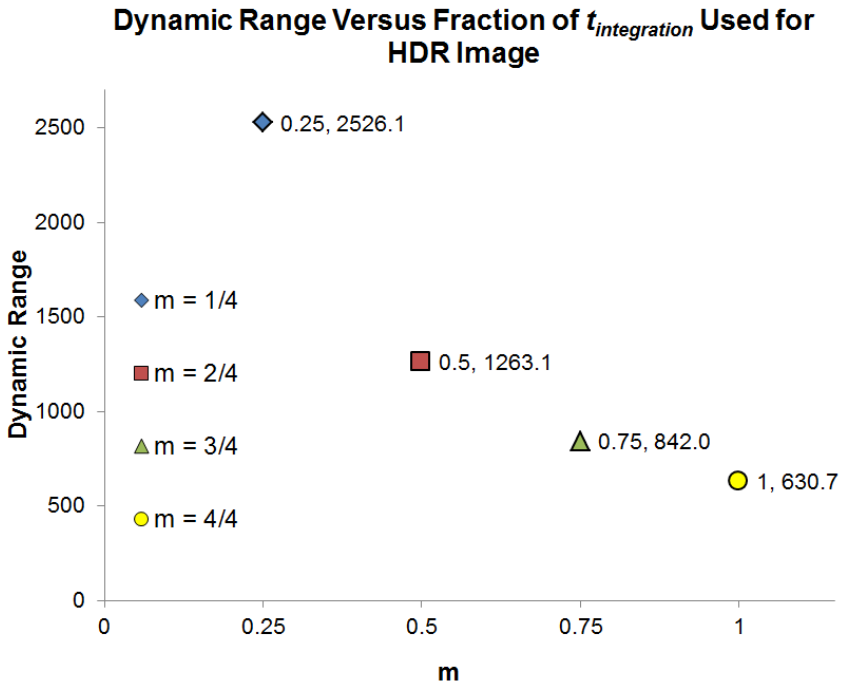

Figure 7. Summary of dynamic range extension results.

5. DISCUSSION

5.1 Comparison with Fowler Sampling and Sample-Up-the-Ramp"

The multiple samples HDR approach has commonalities with astronomy techniques for noise reduction such as Fowler sampling and sample-up-the-ramp (SUTR) since both rely on non-destructive readout to improve sensor performance[21,22]. However the techniques are distinct in common use because the integration times differ substantially (30 fps or higher for HDR versus 1fps or lower for astronomy) and they have different purposes (dynamic range extension versus noise reduction). Fowler sampling and SUTR are used solely to reduce temporal noise by averaging or fitting samples. In Fowler sampling, several non-destructive reads of a pixel are collected and averaged at the beginning of an integration period and a similar number collected and averaged at the end of the integration period. The difference of the two averages is the pixel value with temporal noise reduced. In SUTR, non-destructive samples are taken at uniform spacing over the duration of integration in manner similar to $t_{capture}$ in the multiple samples technique. A linear fit is applied to all samples to determine photocurrent that has reduced temporal noise contribution.

5.2 Future Directions

With multiple samples HDR method verified, the system will be upgraded to process the multiple samples HDR algorithm method in real-time by FPGA, easing burdens on the co-processor. Also, improved memory techniques will allow storage of several thousand consecutive frames. Additional real-time algorithms will be explored, particularly those benefitting high-frame rate applications.

6. CONCLUSION

The multiple samples method works as expected with a representative commercial image sensor, allowing a dynamic range extension proportional to the amount of non-destructive oversampling. Results are adequately modeled by read noise, dark current, and photocurrent.

APPENDIX A: CONVERSION GAIN DERIVATION

Conversion gain allows a user to translate measurements in digital numbers (DN) to electrons (e-). It is the scaling factor that forces measured mean-variance statistics to fit a Poisson distribution. The problem sometimes encountered with the derivation of conversion gain is that the units do not seem to work out. This can be addressed by including a bookkeeping term α, which for a Poisson distribution has the units needed to satisfy

$$\sigma(\bar{s}) = \alpha\sqrt{\bar{s}} \tag{8}$$

Where $\sigma(\bar{s})$ is the standard deviation of the signal (DN or electrons), $\bar{s}$ is the average signal (DN or electrons), and α is the bookkeeping factor ($DN^{1/2}$ or $electrons^{1/2}$). This factor is needed because both σ and $\bar{s}$ must have the same units. Here, σ is a measure of the width of the Poisson distribution in the same units as $\bar{s}$. From here the derivation can proceed as

$$\sigma(\bar{s}_{(DN)}) = \alpha\sqrt{\bar{s}_{(DN)}} \tag{9}$$

$$\sigma_{(DN)} = \alpha\sqrt{\bar{s}_{(DN)}} \tag{10}$$

$$\sigma_{(DN)} K_{(e-/DN)} = \alpha\sqrt{\bar{s}_{(DN)} K_{(e-/DN)}} \tag{11}$$

$$\sigma^2_{(DN)} K^2_{(e-/DN)} = \alpha^2 \bar{s}_{(DN)} K_{(e-/DN)} \tag{12}$$

$$\sigma^2_{(DN)} K_{(e-/DN)} = \alpha^2 \bar{s}_{(DN)} \tag{13}$$

Taking the derivative of both sides with respect to variance, we have

$$K_{(e-/DN)} = \alpha^2 \frac{\partial \bar{s}_{(DN)}}{\partial \sigma^2_{(DN)}} \tag{14}$$

Here, $\frac{\partial \bar{s}_{(DN)}}{\partial \sigma^2_{(DN)}}$ is the slope of the mean-variance plot.

ACKNOWLEDGMENT

We thank Bruce Lambert, Stanley Kohn, and Hung Ngo for contributions to this work. Funding was provided by The Aerospace Corporation through the Internal Research and Development (IR&D) program.

REFERENCES

[1] Spivak, A., Belenky, A., Fish, A., Yadid-Pecht, O., "Wide-dynamic-range CMOS image sensors—comparative performance analysis," IEEE Trans. Electron Devices **56**(11), 2446–2461 (2009).

[2] Kavusi, S., Kakavand, H., El Gamal, A., "Quantitative study of high dynamic range sigma-delta-based focal plane array architectures," Def. Secur., International Society for Optics and Photonics, 341–350 (2004).

[3] Fowler, B., "High dynamic range image sensor architectures," IS&T/SPIE Electron. Imaging, 787602 (2011).

[4] El Gamal, A., Eltoukhy, H., "CMOS image sensors," IEEE Circuits Devices Mag. **21**(3), 6–20 (2005).

[5] Yang, D. X. D., El Gamal, A., "Comparative analysis of SNR for image sensors with enhanced dynamic range," Electron. Imaging, International Society for Optics and Photonics, 197–211 (1999).

[6] Darmont, A., [High Dynamic Range Imaging: Sensors and Architectures], SPIE (2012).

[7] Kavusi, S., "Quantitative study of high-dynamic-range image sensor architectures," Proc. SPIE **5301**, 264–275 (2004).

[8] Posch, C., Matolin, D., Wohlgenannt, R., "A QVGA 143 dB dynamic range frame-free PWM image sensor with lossless pixel-level video compression and time-domain CDS," IEEE J. Solid-State Circuits **46**(1), 259–275 (2011).

[9] Yadid-Pecht, O., Fossum, E. R., "Wide intrascene dynamic range CMOS APS using dual sampling," IEEE Trans. Electron Devices **44**(10), 1721–1723 (1997).

[10] Nakamura, T., Saitoh, K., "Recent progress of CMD imaging," in 1997 IEEE Work. CCDs Adv. Image Sensors, Bruges, Belgium (1997).

[11] Yang, D. X. D., Gamal, A. E., Fowler, B., Tian, H., "A 640×512 CMOS image sensor with ultrawide dynamic range floating-point pixel-level ADC," IEEE J. Solid-State Circuits **34**(12), 1821–1834 (1999).

[12] Liu, X., El Gamal, A., "Synthesis of high dynamic range motion blur free image from multiple captures," Circuits Syst. I Fundam. Theory Appl. IEEE Trans. **50**(4), 530–539 (2003).

[13] Bidermann, W., El Gamal, A., Ewedemi, S., Reyneri, J., Tian, H., Wile, D., Yang, D., "A 0.18 μm high dynamic range NTSC/PAL imaging system-on-chip with embedded DRAM frame buffer," 2003 IEEE Int. Solid-State Circuits Conf. 2003. **1**(June 1997), 212–488 (2003).

[14] Sasaki, M., Mase, M., Kawahito, S., Tadokoro, Y., "A wide-dynamic-range CMOS image sensor based on multiple short exposure-time readout with multiple-resolution column-parallel ADC," IEEE Sens. J. **7**(1), 151–158 (2007).

[15] Bilcu, R. C., Burian, A., Knuutila, A., Vehvilainen, M., "High dynamic range imaging on mobile devices," 2008 15th IEEE Int. Conf. Electron. Circuits Syst., 1312–1315 (2008).

[16] Shang, Y., Guan, Y., Zhang, W., Liu, X., Zhang, S., Zhang, Y., "A high dynamic range complementary metal-oxide-semiconductor (CMOS) camera using multi-slope response and an image reconstruction algorithm," Meas. Sci. Technol. **20**(10), 104005 (2009).

[17] Hasinoff, S. W., Durand, F., Freeman, W. T., "Noise-optimal capture for high dynamic range photography," 2010 IEEE Comput. Soc. Conf. Comput. Vis. Pattern Recognit., 553–560 (2010).

[18] Yasuma, F., Mitsunaga, T., Iso, D., Nayar, S. K., "Generalized assorted pixel camera: postcapture control of resolution, dynamic range, and spectrum.," IEEE Trans. Image Process. **19**(9), 2241–2253 (2010).

[19] Yamada, T., Kasuga, S., Murata, T., Kato, Y., "A 140dB-dynamic-range MOS image sensor with in-pixel multiple-exposure synthesis," IEEE Int. Solid-State Circuits Conf. **35**, 50–594 (2008).

[20] "LUPA 1300.", <http://www.onsemi.com/pub_link/Collateral/NOIL2SM1300A-D.PDF>.

[21] Hoffman, A., Loose, M., Suntharalingham, V., [Scientific Detectors for Astronomy 2005: Explorers of the Photon Odyssey], J. E. Beletic, J. W. Beletic, and P. Amico, Eds., Springer, 377–402 (2006).

[22] McLean, I., [Electronic Imaging in Astronomy], Springer Praxis Books, 412–415 (2008).